CDF/PUB/TOP/PUBLIC/11068

Search for an Invisible Decaying Higgs Boson in Dilepton Events at CDF

M. Bauce, K. Knoepfel, D. Lucchesi, C. Principato[1], G. Punzi, C. Vellidis

The CDF Collaboration, Fermilab

Abstract

We present the first search at the Tevatron for a Higgs boson decaying to an invisible final state. We use the full CDF Run II data set corresponding to 9.7 fb^{-1} of integrated luminosity. We search in the associated ZH production mode and require two same-flavor, oppositely charged leptons and a significant value of missing transverse energy to be in the final state. We exclude values of $\sigma_{ZH\times\mathcal{B}\,(H\to\text{invisible})}$ greater than 90 fb at 95% credibility level for a Higgs boson mass of 125 GeV/c^2. We perform this analysis across a Higgs boson mass range of 115 to 150 GeV/c^2. We are able to exclude a $\mathcal{B}\,(H \to \text{ invisible}) = 100\%$ assumption at Higgs boson masses lower than 120 GeV/c^2.

[1]crisprin@fnal.gov

Contents

1 Introduction

The simplest $H \rightarrow$ invisible process is highly suppressed in the SM. However, beyond-the-SM scenarios allow for enhanced $H \rightarrow$ invisible decay rates that are potentially observable by collider experiments. In this analysis, we search for a $H \rightarrow$ invisible process in the ZH associated production mode. Despite the suppressed cross section relative to gluon fusion, the ZH production mode allows one to trigger on leptonic decays of the Z. For this analysis, we reconstruct Z candidates by combining e^+e^- and $\mu^+\mu^-$ dilepton four-momenta. We do not explicitly reconstruct $Z \rightarrow \tau^+\tau^-$ processes, but as we are not able to infer the missing energy from neutrinos, we gain some acceptance from $\tau^+\tau^-$ decays to same-flavor final states. Events with $e^\pm\mu^\mp$ pairs are used as a control region to test background modeling, as well as events with same-sign, same-flavor lepton pairs. The event selection is described below.

2 Detector Description

The components of the CDF II detector relevant to this analysis are described briefly here; a more complete description can be found elsewhere [1]. The detector geometry is described by the azimuthal angle ϕ and the pseudo-rapidity $\eta \equiv -\ln(tan\theta/2)$, where θ is the polar angle of a particle with respect to the proton beam axis (positive z-axis). The pseudo-rapidity of a particle originating from the center of the detector is referred to as η_{det} . The trajectories of charged particles are reconstructed using silicon microstrip detectors [2, 3] and a 96-layer open- cell drift chamber (COT) [4] embedded in a 1.4 T solenoidal magnetic field. For $\mid \eta_{det} \mid \leq 1$, a particle traverses all 96 layers of the COT; this decreases to zero at $\mid \eta_{det} \mid \approx 2$. The silicon system provides coverage with 6 (7) layers with radii between 2.4 cm and 28 cm for $\mid \eta_{det} \mid < 1.0 (1.0 < \mid \eta_{det} \mid < 2.0)$. Outside of the solenoid are electromagnetic (EM) and hadronic (HAD) sampling calorimeters segmented in a projective tower geometry. The first hadronic interaction length (λ) of the calorimeter, corresponding to 19-21 radiation lengths (X_0), uses lead absorber for measuring the electromagnetic component of showers, while the section extending to 4.5-7 λ uses iron to contain the hadronic component. The calorimeters are divided in a central ($\mid \eta_{det} \mid < 1$) and forward ($1.1 < \mid \eta_{det} \mid < 3.64$) region. Shower maximum detectors (SMX) embedded in the electromagnetic calorimeters at approximately $6X_0$ help in the position measurement and background suppression for electrons. Outside of the central calorimeters are scintillators and drift chambers for identifying muons as minimum ionizing particles. We use three complementary track pattern recognition algorithms which are distinguished by their starting point in COT, silicon, or projection from calorimeter energy cluster to interaction region.

3 Lepton Identification

In order to maximize the signal acceptance and suppress backgrounds from jets and photons misidentified as leptons, we use ten categories of electrons and muons. Two additional categories, based on central tracks that are not fiducial to calorimeters or muon detectors, are used as either an electron or muon in forming $Z \to ll$ candidates. The resulting categories exploit essentially all the tracks and electromagnetic calorimeter clusters available. All leptons are required to be isolated such that the sum of the E_T for the calorimeter towers in a cone of $\sqrt{\Delta\eta^2 + \Delta\phi^2} < 0.4$ around the lepton is less than 10 % of the electron E_T or muon p_T . If an additional good muon or electron candidate is found within the $\Delta R < 0.4$ cone, the towers the additional lepton passed through are subtracted rom the E_T sum. The transverse energy E_T of a shower or calorimeter tower is $Esin\theta$, where E is the associated energy. Similarly, p_T is the component of track momentum transverse to the beam line. Electron candidates are required to have a ratio of HAD energy to EM energy consistent with originating from an electromagnetic shower and are further divided into central and forward categories. The central electron category require a well-measured COT track satisfying $p_T > 10\,\mathrm{GeV}/c$ that is fiducial to the central SMX and matched to a central EM energy cluster. Central electron candidates are then selected using a likelihood method to combine electron identification variables into one discriminant. A forward electron is required to be fiducial to the forward SMX detector and have energy deposition in both the calorimeter towers and SMX detector consistent with an electron shower shape. For each forward candidate, we also require a matching calorimeter seeded track that is consistent with a standalone reconstructed track formed using hits in the silicon detector, to reduce background from photons. If a forward electron fails this cut based category, it has a chance to pass using likelihood based discriminant. Muons are identified by either a charged track matched to a reconstructed track segment (stub) in muon chambers or as a stubless minimum ionizing particle fiducial to calorimeters. In addition, stubless muons are required to have at least 0.1 GeV in total calorimeter energy. For $\eta_{det} < 1.2$, strict requirements on the number of COT hits and the χ^2 of the track fit are placed on the muon tracks in order to suppress kaon decay-in-flight backgrounds. The category of stubless muons with $\mid \eta_{det} \mid > 1.2$ requires that at least 60% of the COT layers crossed by the track have hits. In order to suppress background from cosmic rays, the track's point of closest approach to the beam-line must be consistent with originating from the beam. The final category of leptons are constructed from tracks which are not fiducial to the SMX detectors nor identified as stubbed muons. The requirements for the tracks are the same as stubless muons with $\mid \eta_{det} \mid < 1.2$, but without any of the calorimeter requirements. Due to the lack of calorimeter information, electron and muons cannot be reliably differentiated in this region, and this category is therefore treated as having either flavor in the Z candidate selection. If an electron or non-fiducial track candidate is consistent with being due to a photon conversion as indicated by the presence of an additional nearby track, the candidate is vetoed.

To identify the presence of neutrinos, we define the missing transverse energy $\not\!\!E_T$=|

$\sum_i E_{T,i} \cdot \widehat{n_{T,i}}$ |, where the $\widehat{n_{T,i}}$ is the transverse component of the unit vector pointing from the interaction point to the calorimeter tower i.

The $\not\!\!E_T$is corrected for muons which do not deposit all of their energy in the calorimeter and tracks which point to uninstrumented regions of the calorimeter. The ZZ candidate events are required to pass one of five online trigger selections implemented in three successively more stringent levels. The final central electron requirement is EM energy cluster with $E_T > 18$ GeV matched to a track with $p_T > 8\,\mathrm{GeV}/c$. Muon triggers are based on information from muon chambers matched to a track with $p_T > 18\,\mathrm{GeV}/c$. Selection efficiencies are measured in data and MC simulation using $Z \to ll$ samples. Correction factors are then applied to each process simulation obtained from the ratio of the efficiency calculated in the simulation and in the data.

4 Event selection

Events are collected using high-p_T muon and high-E_T electron triggers. We require the final state in the signal region to have exactly two same-flavor, oppositely charged leptons. Electrons are identified as objects that have a high-momentum track that deposits almost all of its energy in the electromagnetic compartment of the calorimeter. Muons are identified by matching signatures in the outer muon detectors with tracks made in the inner tracking detector. We consider many combinations of leptons based on which subdetector recorded them; as well as combinations of reconstructed leptons with reconstructed tracks that could not be unambiguously identified as electrons or muons.

In order to suppress backgrounds, we require various event-selection criteria:

- The dilepton transverse momentum must be at least 45 GeV/c
- We accept no events where a reconstructed jet with $E_T \geq$15 GeV satisfies $\Delta\phi(ll, J) \geq$ 2.0 radians
- The azimuthal separation between the $\not\!\!E_T$and closest leading lepton must be at least 0.5 radians

Additional requirements, described below, are imposed depending on the control region or signal region.

5 Data Modeling

The expectation and modeling of signal and background processes are determined using different Monte Carlo (MC) simulations including a GEANT-based simulation of the CDF II detector [5]; CTEQ5L parton distribution functions (PDFs) are used to model the momentum distribution of the initial-state partons [6]. The WZ, ZZ, Z+jets, and $t\bar{t}$ processes are simulated using PHYTIA [7] while $WW$is simulated using MC@NLO

[8]. $W\gamma$ background is modeled with the Baur event generator [9]. Each simulated sample is normalized to the theoretical cross section calculated at next-to-leading order in QCD using [10]. W+jets background is data driven. For the Z+jets background, we normalize the prediction to the data by a factor of $sf = 1.7 \pm 5\%$ (subtracted of all other backgrounds) in the region from 0 $<\not\!\!E_T<$ 40 GeV, where all event selection requirements have been made except the $\not\!\!E_T>$ 60 GeV criterion. After this multiplicative correction is made, a (+3 $\pm$ 33%) GeV correction in the $\not\!\!E_T$value is applied only for Z+jets events, to bring the corresponding $\not\!\!E_T$distribution into better agreement with that of background-subtracted data.

5.0.1 Signal Region definition

For the signal region, we additionally require:

- Reconstructed $l^{\pm}l^{\pm}$ dilepton pair, where l is an electron or muon
- Dilepton invariant mass that lies in the union $82 < M_{ll} < 100$ GeV/c^2
- Azimuthal separation between the $\not\!\!E_T$and closest leading lepton to be at least 0.5 radians
- Missing transverse energy of at least 60 GeV

The event yields in the signal region are listed in Table [1]:

Table 1: Expected and observed number of events passing the kinematic requirements defining the signal region

$ZH \rightarrow \mathbf{l^+l^-}$ + **invisible** (signal region) CDF Run II Preliminary, $\mathcal{L}$=9.1fb^{-1}	
ZZ	27.2 $\pm$ 2.9
WW	19.2 $\pm$ 1.8
WZ	13.7 $\pm$ 1.5
Z+jets	7.1 $\pm$ 3.1
W+jets	3.8 $\pm$ 0.6
$t\bar{t}$	5.5 $\pm$ 0.9
$W\gamma$	0.5 $\pm$ 0.1
Total prediction	76.9 $\pm$ 7.2
Data	78
ZH (m_H = 125 GeV/c^2)	8.2 $\pm$ 1.3

The uncertainties on the total prediction include the correlations between the various systematic uncertainties that are taken into account (and described below Sec[5.2]).

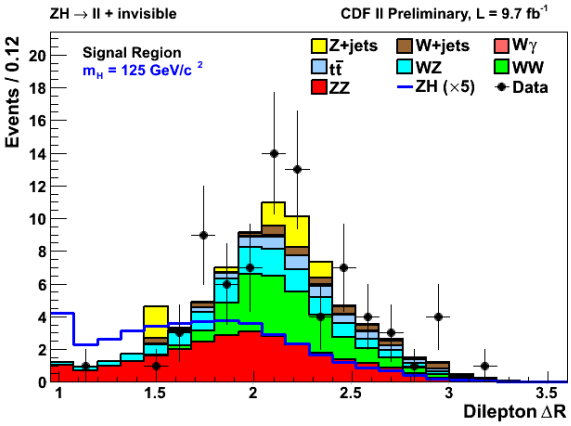

(a) $\Delta R(ll)$ between leptons

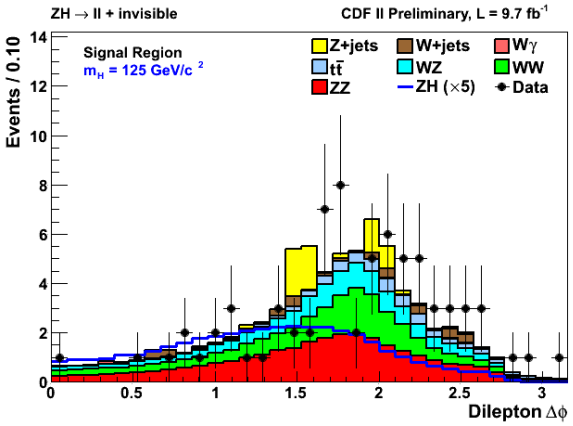

(b) $\Delta\phi(ll)$ between leptons

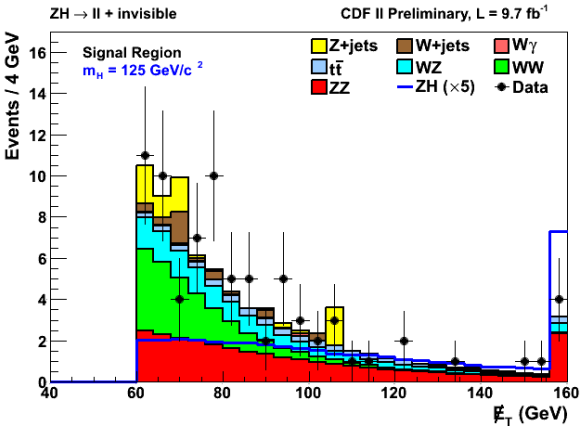

(c) Missing Transverse Energy

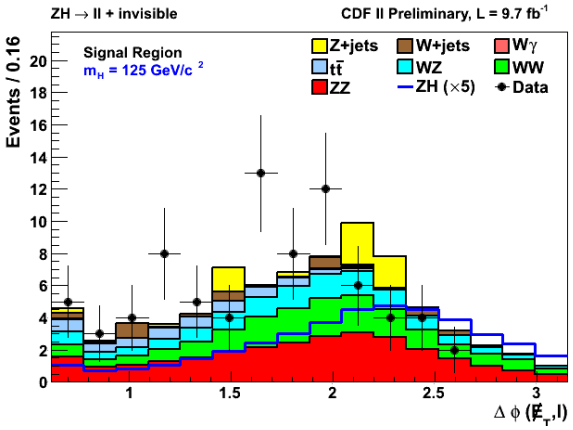

(d) $\Delta\phi$ between $\not\!\!E_T$and leading lepton

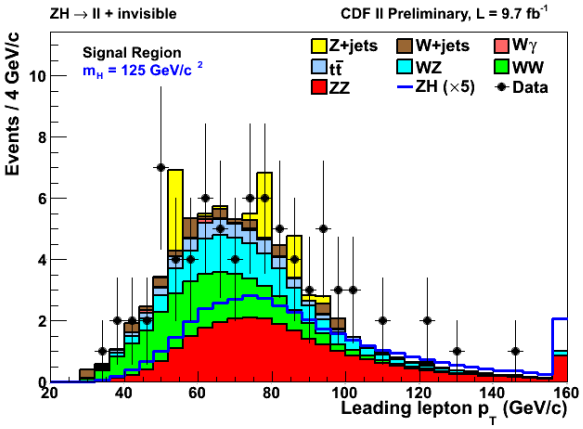

(e) Transverse momentum of leading lepton

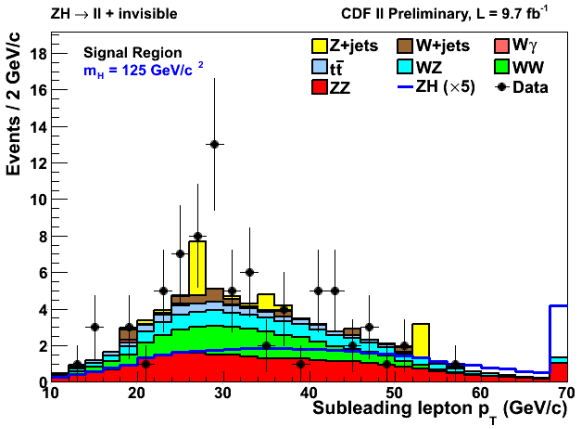

(f) Transverse momentum of subleading lepton

Figure 1: Signal region

5.1 Background model validation

This model is tested and validated in three control regions:

- An opposite flavor, opposite sign ($e^{\pm}\mu^{\mp}$) control region
- A same-sign, same-flavor control region
- A same-flavor, opposite-sign, sideband (in dilepton invariant mass) control region

For each of these control regions, we provide validation plots for six variables:

- The missing transverse energy of the event - $\not{E}_T$
- The azimuthal angle between the $\not{E}_T$vector and the closest leading lepton l - $\Delta\phi(\not{E}_T, l)$
- $\Delta R(ll)$ between the leading leptons
- Dilepton transverse momentum - $p_T(ll)$
- Leading lepton transverse momentum
- Subleading lepton transverse momentum

The control regions are defined more explicitly below. For each control region including the signal region, the default event-selection requirements as mentioned above are imposed. As can be seen, the background model agrees well with data.

5.1.1 Opposite-flavor, opposite-sign control region

For the opposite flavor, opposite control region, we additionally require:

- Reconstructed $e^{\pm}\mu^{\mp}$ dilepton pair
- Dilepton invariant mass within the range $40 \leq M_{ll} \leq 140$ GeV/c^2
- Missing transverse energy of at least 20 GeV ($\not{E}_T$plot below truncates at 40 GeV, including lower-$\not{E}_T$events in the first bin of the plot)

The event yields in the opposite-flavor, opposite-sign control region are listed in Table [2]:

The uncertainties on the total prediction include the correlations between the various systematic uncertainties that are taken into account (and described below).

Table 2: Expected and observed number of events passing the kinematic requirements defining the opposite flavor, opposite sign control region

$ZH \to \ell^+\ell^- +$ **invisible** ($e^\pm\mu^\mp$ control region) CDF Run II Preliminary, $\mathcal{L} = 9.7$ fb^{-1}	
ZZ	0.17 ± 0.02
WW	96.4 ± 8.9
WZ	2.4 ± 0.3
Z +jets	9.3 ± 4.1
W+jets	24.2 ± 3.6
$t\bar{t}$	14.2 ± 2.3
$W\gamma$	16.9 ± 2.8
Total prediction	163.7 ± 12.6
Data	155

5.1.2 Same-sign control region

For the same sign control region, we additionally require:

- Reconstructed $l^\pm l^\pm$ dilepton pair, where l is an electron or muon
- Dilepton invariant mass within the range $40 \leq M_{ll} \leq 140$ GeV/c^2
- Missing transverse energy of at least 40 GeV

The event yields in the same-sign, same-flavor control region are listed in Table [3] :

Table 3: Expected and observed number of events passing the kinematic requirements defining the same-sign, same-flavor control region

$ZH \to \ell^+\ell^- +$ **invisible** (same-sign control region) CDF Run II Preliminary, $\mathcal{L} = 9.7$ fb^{-1}	
ZZ	0.66 ± 0.07
WW	1.7 ± 0.2
WZ	7.2 ± 0.8
Z +jets	2.9 ± 1.3
W+jets	30.1 ± 4.5
$t\bar{t}$	0.22 ± 0.04
$W\gamma$	8.4 ± 1.4
Total prediction	51.1 ± 5.1
Data	57

The uncertainties on the total prediction include the correlations between the various systematic uncertainties that are taken into account (and described below).

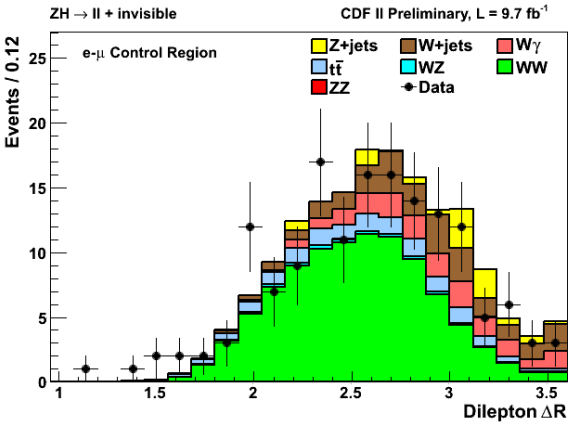

(a) $\Delta R(ll)$ between leptons

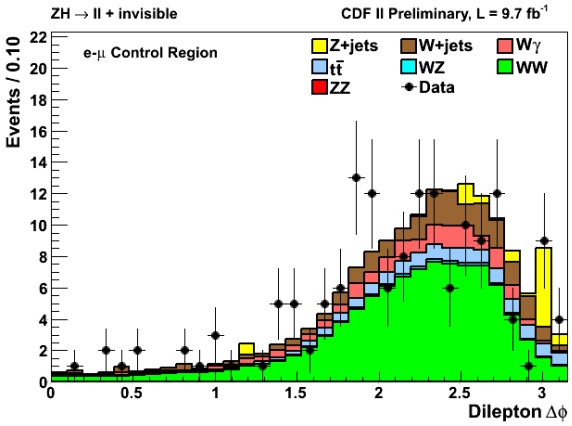

(b) $\Delta\phi(ll)$ between leptons

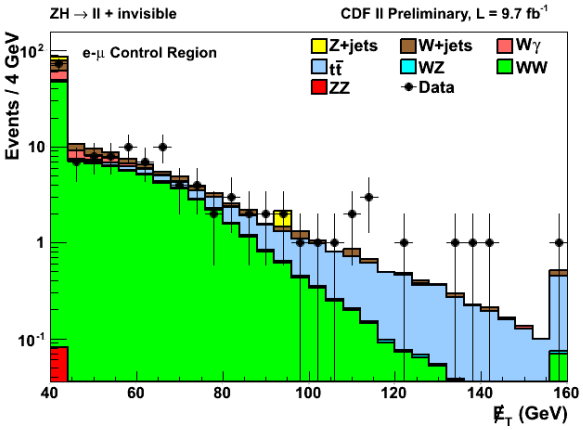

(c) Missing Transverse Energy

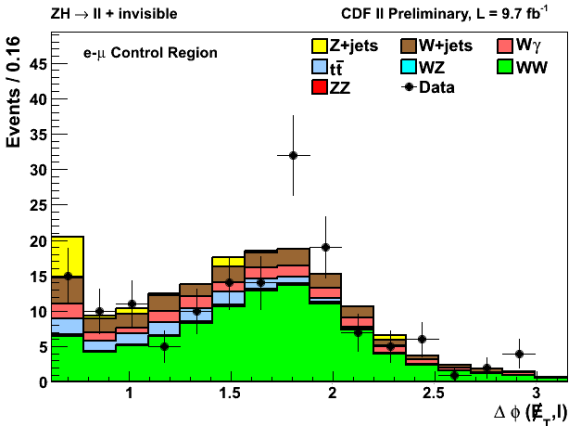

(d) $\Delta\phi$ between $\not\!\!E_T$and leading lepton

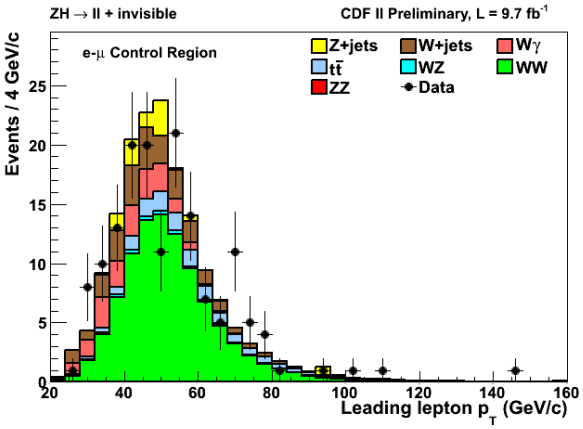

(e) Transverse momentum of leading lepton

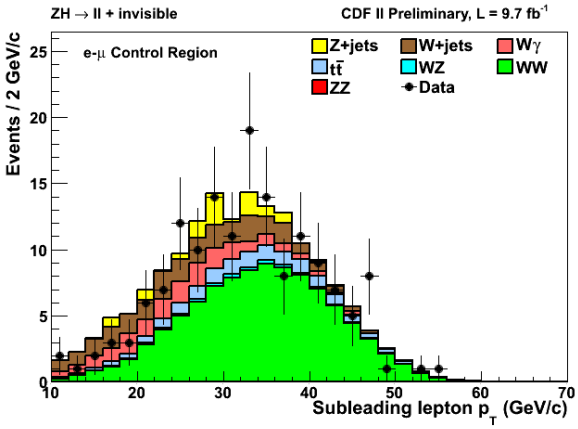

(f) Transverse momentum of subleading lepton

Figure 2: Opposite-flavor, opposite-sign control region

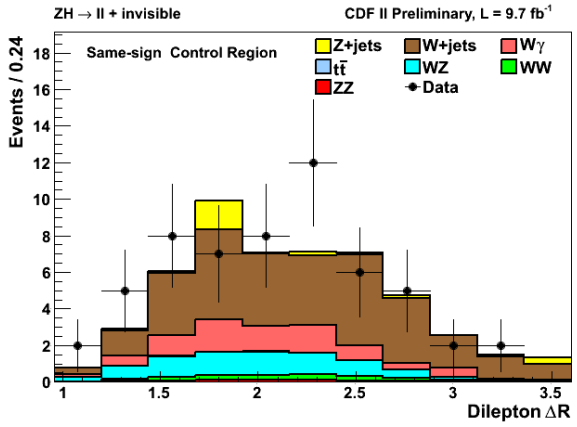

(a) $\Delta R(ll)$ between leptons

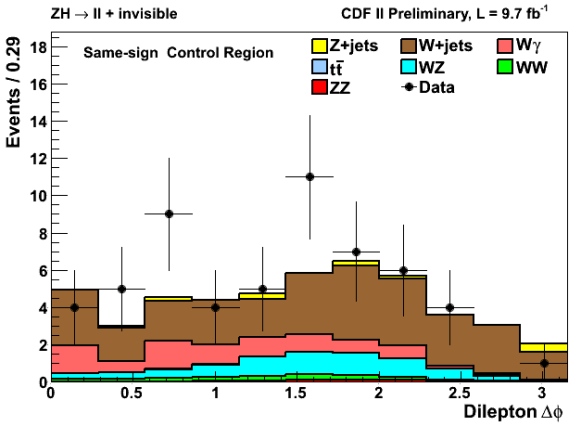

(b) $\Delta\phi(ll)$ between leptons

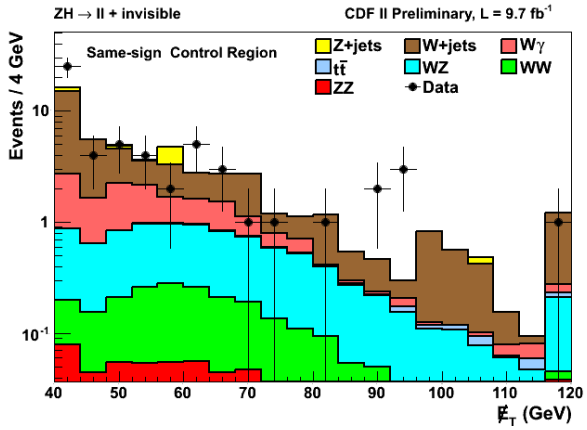

(c) Missing Transverse Energy

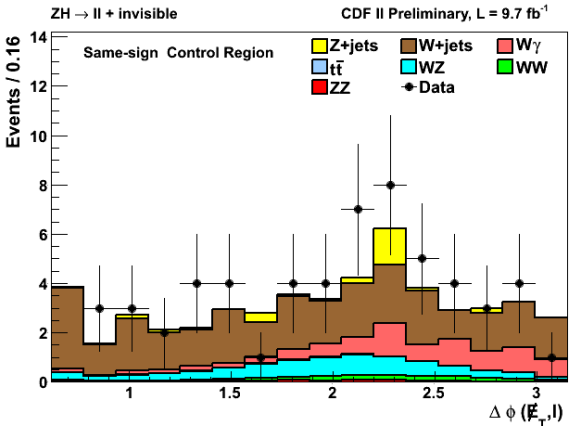

(d) $\Delta\phi$ between $\not\!\!E_T$ and leading lepton

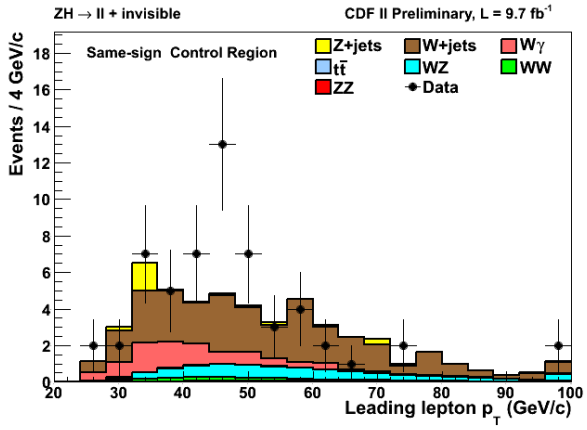

(e) Transverse momentum of leading lepton

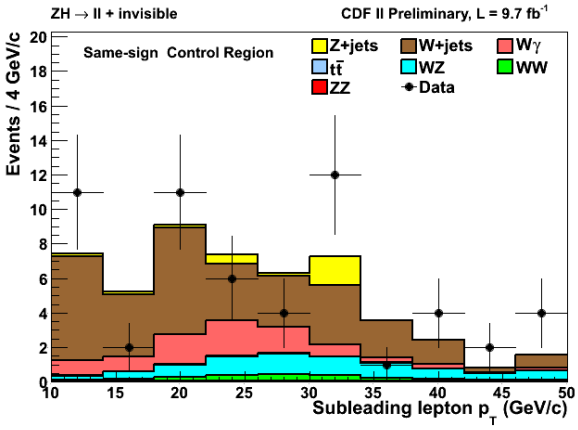

(f) Transverse momentum of subleading lepton

Figure 3: Same-sign, same-flavor control region

5.1.3 Sideband control region

For the sideband control region, we additionally require:

- Reconstructed $l^{\pm}l^{\pm}$ dilepton pair, where l is an electron or muon
- Dilepton invariant mass that lies in the union $[50, 82] \cup [100, 132]\text{GeV}/c^2$
- Missing transverse energy of at least 50 GeV

The event yields in the sideband control region are listed in Table [4]:

Table 4: Expected and observed number of events passing the kinematic requirements defining the sideband control region

$\boldsymbol{ZH \to \ell^+\ell^- +}$ **invisible** (sideband control region) CDF Run II Preliminary, $\mathcal{L} = 9.7$ fb^{-1}	
ZZ	6.2 ± 0.7
WW	113.4 ± 10.4
WZ	5.2 ± 0.6
Z +jets	1.7 ± 0.7
W+jets	19.8 ± 3.0
$t\bar{t}$	20.1 ± 3.3
$W\gamma$	6.2 ± 1.0
Total prediction	172.7 ± 13.7
Data	177

The uncertainties on the total prediction include the correlations between the various systematic uncertainties that are taken into account (and described below).

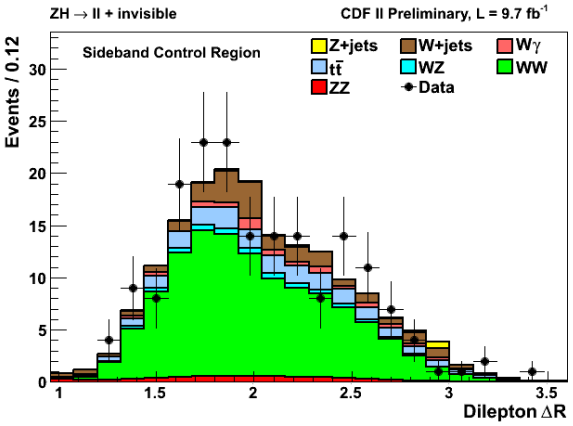

(a) $\Delta R(ll)$ between leptons

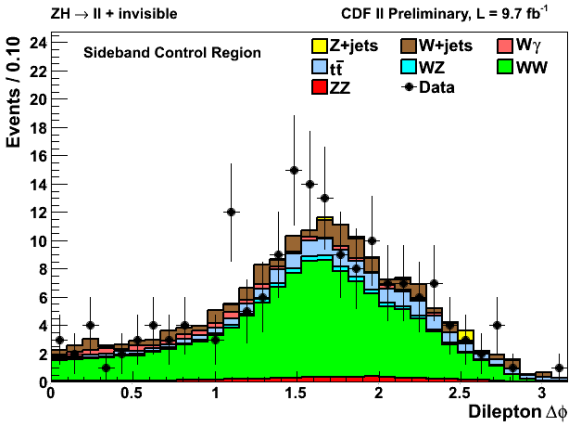

(b) $\Delta\phi(ll)$ between leptons

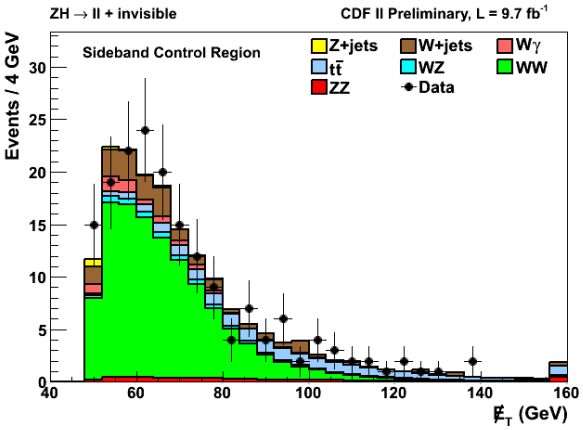

(c) Missing Transverse Energy

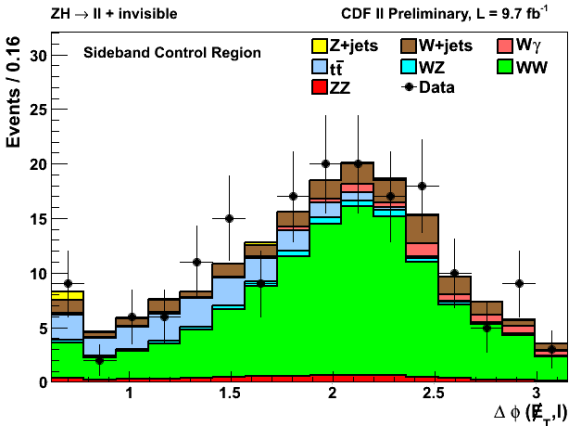

(d) $\Delta\phi$ between $\not\!\!E_T$ and leading lepton

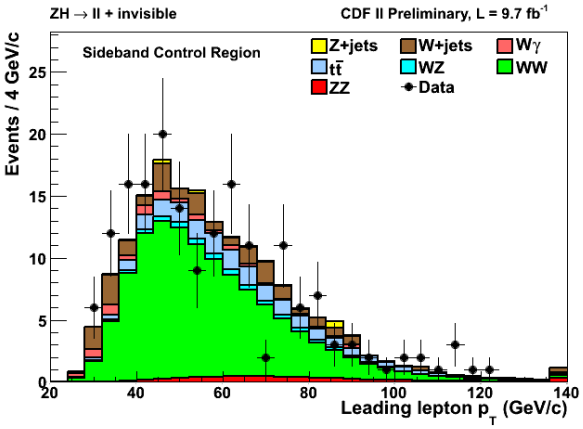

(e) Transverse momentum of leading lepton

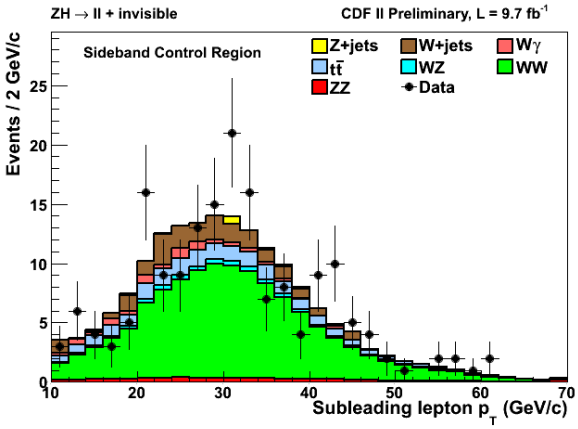

(f) Transverse momentum of subleading lepton

Figure 4: Sideband M_{ll} $[50, 82] \cup [100, 132]\text{GeV}/c^2$ control region

5.2 Systematic uncertainties

We take into account various systematic uncertainties by introducing nuisance parameters that are typically described using Gaussian distributions, centered at the central value of the systematic correction, with a root-mean-square width equal to its one-standard-deviation value. If necessary, the Gaussian is truncated at zero to avoid negative event yields when running pseudo-experiments. The values of the uncertainties used are shown here in Table [5] :

Table 5: Table of the Systematic uncertainties considered in the measurement

$ZH \to \ell^+\ell^- +$ **invisible**	CDF Run II Preliminary, $\mathcal{L} = 9.7$ fb^{-1}							
Systematic Uncertainties (%)	ZZ	WZ	WW	$t\bar{t}$	W+jets	Z+jets	$W\gamma$	ZH
Theory cross section	6	6	6	10		33	10	5
NLO acceptance	5	5		10			5	10
Luminosity	5.9	5.9	5.9	5.9			5.9	5.9
Electron conversion							10	5.9
Jet-energy scale	2	4	1	4		28	3	1
Initial/final state radiation								8
Fake lepton rate					15			
Lepton ID	3	3	3	3		3		3
Trigger efficiency	2	2	2	2		2		2

As the W/Z+jets samples are largely derived from data, many of the systematic uncertainties common to the other samples are not applicable. Note also that the primary effects that could cause a shape variation in the final discriminant are the jet-energy scale, and initial- and final-state radiation. Because we do not cut explicitly on the number of jets in the final state, but rather we veto an event if a jet is in relative proximity with the $\not\!\!E_T$vector, the jet-energy scale and gluon radiation effects translate to rate uncertainties. Therefore, we include no variations in the $\Delta R(ll)$ shape in our treatment of the systematic uncertainties.

6 Results

Results are obtained by constructing a likelihood function that is the product of Poisson probabilities for each bin of the $\Delta R(ll)$ distribution. The sensitivity of the analysis to excluding the Higgs boson signal is degraded by accounting for systematic uncertainties, as described above. This is included by scaling the likelihood by each of the nuisance-parameter prior probability densities, which are truncated when necessary to ensure non-negative event yields. To estimate the sensitivity of the analysis, we run many pseudo-experiments by drawing random combinations of nuisance parameter values from the prior probability densities. As we are testing to exclude a hypothesis (the presence of ZH, where $H \rightarrow$invisible), we include no signal contributions to the mean values of the Poisson probabilities. We use a non-negative uniform prior for the signal strength R, which is the ratio between the observed and assumed signal cross sections. The upper limit R_{95} is obtained by integrating over all nuisance parameters except for R and finding location of the posterior probability that corresponds to an integral of 95%.

This procedure is repeated for each pseudo-experiment, and the median and 1- and 2-standard deviation variations of the resulting R_{95} distribution are extracted, where the median represents the expected overall sensitivity to excluding the signal hypothesis. Finally, this procedure is performed for data, where a single value of R_{95} is determined. This process is done for each assumed Higgs boson mass.

The upper limits, given relative to the assumed cross section, are shown in the table below [6]:

Table 6: Table of the upper limits, given relative to the assumed cross section

$\boldsymbol{ZH \rightarrow \ell^+\ell^- +}$ **invisible**	CDF Run II Preliminary, $\mathcal{L} = 9.7$ fb^{-1}					
m_H (GeV/c^2)	95% C.L. on $\sigma_{ZH} \times \mathcal{B}(H \rightarrow \text{invisible})/\sigma_{ZH,\text{SM}}$					
	-2 s.d.	-1 s.d.	**Exp.**	+1 s.d.	+2 s.d.	**Obs.**
115	0.73	1.19	**1.82**	2.81	4.37	**0.93**
120	0.79	1.29	**1.97**	3.04	4.78	**0.97**
125	0.84	1.37	**2.10**	3.26	5.08	**1.04**
130	0.90	1.46	**2.23**	3.47	5.47	**1.16**
135	0.95	1.53	**2.35**	3.64	5.77	**1.17**
140	1.03	1.65	**2.52**	3.91	6.18	**1.26**
145	1.09	1.75	**2.67**	4.16	6.64	**1.38**
150	1.15	1.85	**2.82**	4.38	6.97	**1.37**

The $\pm$1 and $\pm$2-s.d. columns refer to the $\pm$1- and $\pm$2-standard deviation bands as described above. The normalization of the signal is chosen such that $\mathcal{B}$ ($H \rightarrow$ invisible) =100%. Hence any observed limit that lies below a limit of 1 excludes $\mathcal{B}$ ($H \rightarrow$ invisible) =100% at 95% credibility level. The same results are plotted here:

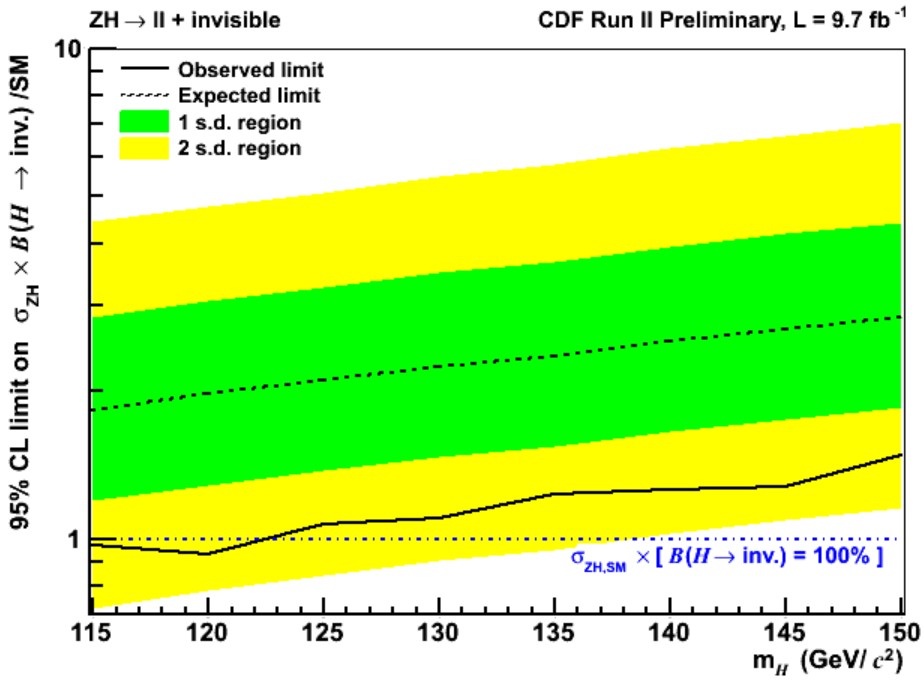

Figure 5: 95% credibility limits for Higgs boson production normalized to the assumed prediction for $\sigma_{ZH,\mathrm{SM}} \times \mathcal{B}(H \rightarrow \text{invisible})$. The branching ratio is assumed to be 100%, whereas the production cross section is assumed to be the SM prediction for ZH production.

The limits can be renormalized such that the $\mathcal{B}(H \rightarrow \text{invisible})$ =100% assumption is removed, and we place a upper limits on $\mathcal{B}(H \rightarrow \text{invisible})$ itself. To do this, we do not include the uncertainty on the ZH theoretical uncertainty as the ZH signal no longer serves as the normalization factor: We therefore exclude cross section values of $H \rightarrow$ invisible, produced in association with $Z \rightarrow l^+l^-$, smaller than 90 fb at a Higgs boson mass of 125 GeV/c^2.

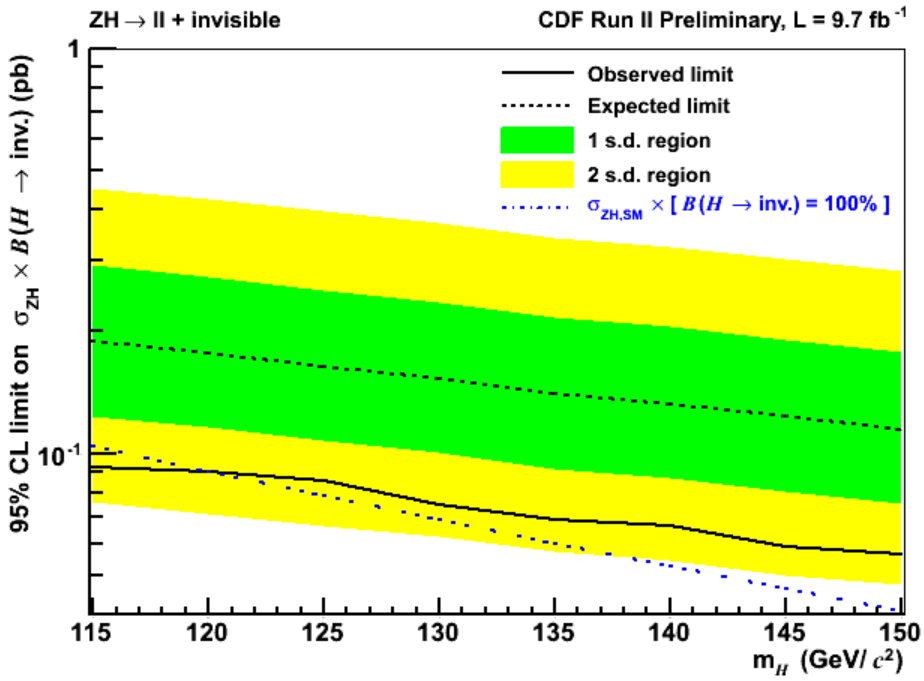

Figure 6: 95% credibility limits for $\sigma_{ZH} \times \mathcal{B}(H \to \text{invisible})$. No assumption on the cross section or branching ratio is made for the expected and observed results. The SM prediction assuming $H \to$ invisible branching ratio of 100% is also shown.

References

[1] R. Blair et al., (CDF Collaboration) (1996), FERMILAB-PUB-96/390-E.

[2] A. Sill et al., Nucl. Instrum. Methods A **447**, 1 (2000).

[3] A. Affolder et al., Nucl. Instrum. Methods A **453**, 84 (2000).

[4] T. Affolder et al., Nucl. Instrum. Methods A **526**, 249 (2004).

[5] R. Brun et al., version 3.15, CERN-DD-78-2-REV.

[6] H. L. Lai et al. (CTEQ), Eur. Phys. J. **C12**, 375 (2000).

[7] T. Sjostrand, S. Mrenna, and P. Skands, JHEP **05**, 026 (2006).

[8] S. Frixione and B. R. Webber, JHEP **06** (2002), hep-ph/0204244.

[9] U. Baur and E. L. Berger, Phys. Rev. D **47**, 4889 (1993).

[10] J. Campbell and R. K. Ellis, MCFM - Monte Carlo for FeMtobarn processes (2010), We ran MCFM Monte Carlo with the MSTW2008 PDF set and varying the factorizzation and renormalizzation scale.

[11] S.-C. Hsu, Ph.D. thesis, UC, San Diego (2008), FERMILAB-THESIS-2008-61.

[12] M. Feindtz and U. Kerzel, Nucl. Instr. Meth. **A**, 190 (2006).

[13] S. Kretzer, H. L. Lai, F. I. Olness, and W. K. Tung, Phys. Rev. D **69**, 114005 (2004).

[14] D. Acosta et al., Nucl. Instrum. Meth. A **494**, 57 (2002).

[15] J. Campbell and R. K. Ellis, Phys. Rev. D **60**, 113006 (1999).

[16] U. Baur, T. Han, and J. Ohnemus, Phys. Rev. D **57**, 2823 (1998).

[17] N. Kidonakis and R. Vogt, Phys. Rev. D **68**, 114014 (2003).

[18] M. Cacciari, S. Frixione, M. L. Mangano, P. Nason, and G. Ridolfi, JHEP **04**, 068 (2004).

7 Acknowledgments

We thank the Fermilab staff and the technical staffs of the participating institutions for their vital contributions. This work was supported by the U.S. Department of Energy and National Science Foundation; the Italian Istituto Nazionale di Fisica Nucleare; the Ministry of Education, Culture, Sports, Science and Technology of Japan; the Natural Sciences and Engineering Research Council of Canada; the National Science Council of the Republic of China; the Swiss National Science Foundation; the A.P. Sloan Foundation; the Bundesministerium für Bildung und Forschung, Germany; the Korean World Class University Program, the National Research Foundation of Korea; the Science and Technology Facilities Council and the Royal Society, United Kingdom; the Russian Foundation for Basic Research; the Ministerio de Ciencia e Innovación, and Programa Consolider-Ingenio 2010, Spain; the Slovak R&D Agency; the Academy of Finland; the Australian Research Council (ARC); and the EU community Marie Curie Fellowship Contract No. 302103.